COMMUNICATIONS

Magnetic Resonance in Medicine 46:419–423 (2001)

Proteoglycan-Induced Changes in $T_{1\rho}$-Relaxation of Articular Cartilage at 4T

Sarma V.S. Akella,[1*] Ravinder Reddy Regatte,[1] Alexander J. Gougoutas,[1] Arijitt Borthakur,[1] Erik M. Shapiro,[2] J. Bruce Kneeland,[1] John S. Leigh,[1] and Ravinder Reddy[1]

Proteoglycan (PG) depletion-induced changes in $T_{1\rho}$ (spin-lattice relaxation in rotating frame) relaxation and dispersion in articular cartilage were studied at 4T. Using a spin-lock cluster pre-encoded fast spin echo sequence, $T_{1\rho}$ maps of healthy bovine specimens and specimens that were subjected to PG depletion were computed at varying spin-lock frequencies. Sequential PG depletion was induced by trypsinization of cartilage for varying amounts of time. Results demonstrated that over 50% depletion of PG from bovine articular cartilage resulted in average $T_{1\rho}$ increases from 110–170 ms. Regression analysis of the data showed a strong correlation ($R^2 = 0.987$) between changes in PG and $T_{1\rho}$. $T_{1\rho}$ values were highest at the superficial zone and decreased gradually in the middle zone and again showed an increasing trend in the region near the subchondral bone. The potentials of this method in detecting early degenerative changes of cartilage are discussed. Also, $T_{1\rho}$-dispersion changes as a function of PG depletion are described. Magn Reson Med 46:419–423, 2001. © 2001 Wiley-Liss, Inc.

Key words: MRI; osteoarthritis; cartilage; $T_{1\rho}$-relaxation

Articular cartilage is a dense, avascular connective tissue whose extracellular matrix (ECM) is a framework of collagen fibers, proteoglycan (PG) aggregates, noncollagenous proteins, and water (1). Water content in cartilage ranges from 66–79% (2). Approximately 60% of the dry weight of cartilage is collagen, with the majority of the remaining portion being PG (3). PG is nonuniformly distributed within the cartilage, with an increased amount present in the center of the matrix and low amounts in the peripheries (4). PG is largely responsible for the high elasticity and resilience of the tissue. It consists of a central protein core to which a large number of negatively charged glycosaminoglycan (GAG) sidechains are covalently attached (5–7). The GAG molecules consist of long chain unbranched repeating dimeric polysaccharides, the most common of these being chondroitin-4-sulfate, chondroitin-6-sulfate, and keratan sulfate. The negatively charged side groups of polysaccharides, sulfates, and carboxylates within the PG impart a fixed charge density (FCD) to the cartilage (8–10). This highly negatively charged environment of PG draws sodium ions into the framework to maintain overall electroneutrality. The swelling pressure generated by sodium ions allows cartilage to maintain its form and durability.

The loss of PG is an initiating event in the early stages of osteoarthritis (OA) (11,12). However, in the early stages of OA the amount of collagen in the framework does not seem to be severely affected. Conventional proton MRI techniques such as T_1-, T_2-, and magnetization transfer (MT)-weighted imaging have been shown to be inconclusive in detecting early changes in OA (13–16). Recent work on delayed gadolinium (Gd)-enhanced MRI of cartilage (dGEMRIC) (17,18) and sodium MRI (19,20) have shown that it is possible to measure PG changes in cartilage both in vivo and in vitro. However, the dGEMRIC method, despite its advantages, requires intravenous injection of contrast agent, a significant delay of at least 2 hr before T_1 map can be obtained, and it also requires joint exercise after the injection of the contrast agent for penetration of $Gd(DTPA)^{2-}$ into the cartilage. Also, there is the need for accurate measurements of intratissue $Gd(DTPA)^{2-}$ relaxivity (21). Sodium MRI, despite its high specificity towards PG, has inherently low sensitivity and requires special hardware modifications.

Spin lattice relaxation in the rotating frame ($T_{1\rho}$)-weighted imaging is an attractive alternative to the existing MRI methods. It is well suited for probing macromolecular slow motions at high static fields (22,23). $T_{1\rho}$-imaging has been shown to be sensitive to changes in PG of cartilage (24). On human cartilage specimens obtained following knee replacement surgery, T_2 and $T_{1\rho}$ have been found to increase substantially (25). However, there has been no systematic study to provide information on the dependence of $T_{1\rho}$ and its dispersion on PG content of cartilage. This information is a prerequisite for using $T_{1\rho}$-weighted imaging for quantifying PG-induced changes in healthy as well as degenerated cartilage.

The purpose of this article is to quantify PG-induced changes in $T_{1\rho}$ relaxation and dispersion in articular cartilage at 4T. Results from bovine articular cartilage demonstrate that $T_{1\rho}$-relaxation times increase almost linearly with PG depletion.

MATERIALS AND METHODS

$T_{1\rho}$-weighted imaging experiments were performed on a 4T whole-body GE Signa scanner (General Electric, Mil-

[1]Department of Radiology Stellar-Chance Laboratories, University of Pennsylvania Medical Center, Philadelphia, Pennsylvania.

[2]Department of Chemistry, University of Pennsylvania Medical Center, Philadelphia, Pennsylvania.

Grant sponsor: NIH; Grant number: RR02305; Grant sponsor: National Institutes of Arthritis and Musculoskeletal & Skin Diseases; Grant numbers: R01-AR45242; R01-AR45404.

*Correspondence to: Sarma V.S. Akella, Ph.D., MMRRCC, Department of Radiology, B1, Stellar-Chance Laboratories, 422 Curie Boulevard, University of Pennsylvania Medical Center, Philadelphia, PA 19104-6100. E-mail: sarma@mail.mmrrcc.upenn.edu

Received 5 March 2001; revised 2 May 2001; accepted 16 May 2001.

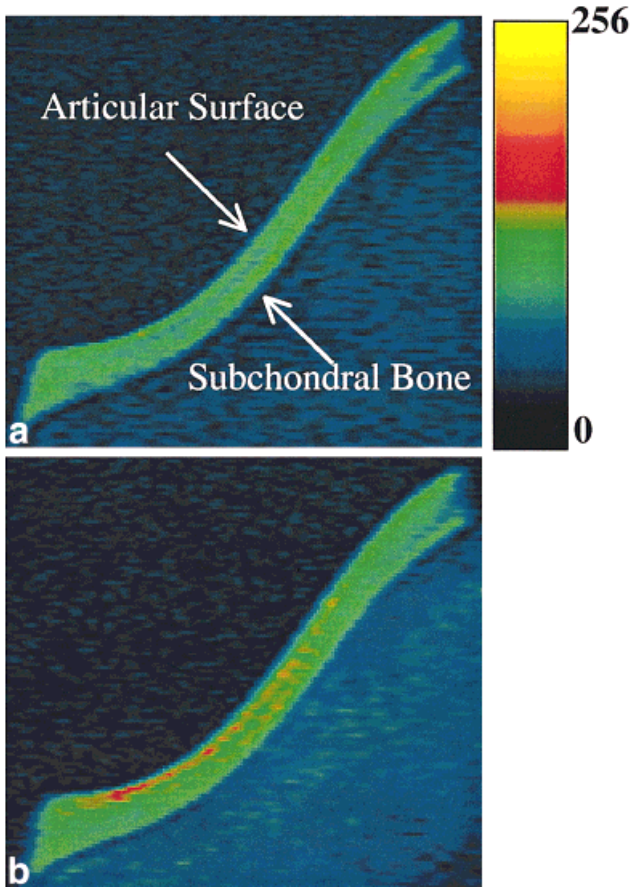

FIG. 1. T_2 and $T_{1\rho}$-weighted images of a healthy bovine patella. **a:** T_2-weighted image obtained with a TE/TR = 80 ms/4 sec; FOV = 7 × 7 cm; slice thickness = 3 mm; matrix = 512 × 128; NEX = 1. **b:** $T_{1\rho}$-weighted image obtained with a B_1 field of 750 Hz; TE + TSL = 80 ms; TR = 4 sec; FOV = 7 × 7 cm; slice thickness = 3 mm; matrix = 512 × 128; NEX = 1.

waukee, WI). An 11-cm diameter birdcage coil tuned to 170 MHz was employed for $T_{1\rho}$ imaging. Fresh bovine patellae were obtained from a slaughterhouse (Bierig Bros., NJ) within 24 hr postmortem. The extraneous tissue (ligaments, fat, etc.) was cut away with a scalpel before proceeding to the experiment. A groove was made in the middle of the patella on the articular surface. The patellae were placed in a chamber containing a nonpermeable divider such that the groove was wedged on the divider. One side of the patella was equilibrated in 137 mM phosphate buffered saline (PBS) and the other side of the patella was immersed in fresh degradation media containing 0.1 mg/ml trypsin in PBS (26). Initially, $T_{1\rho}$-imaging and spin-echo imaging were performed on healthy patellae before degradation. The specimens were placed in the degradation media following these initial experiments. Every 2 hr, the patellae were removed from the media and washed with PBS and $T_{1\rho}$-imaging was performed. A total of five patellae were studied. After the imaging, patellae were returned to fresh degradation media. The degradation and imaging process continued for 6 hr, with imaging performed every 2 hr. This procedure allowed the evaluation of sequential PG loss with $T_{1\rho}$-imaging. The PG extruded in the medium was assayed using 1,9 dimethyl methylene blue (DMMB) dye binding spectrophotometric assay to measure the concentration of PG, as described previously (27). The absorbance was read at 535 nm. The standard curve was made with chondroitin sulfate.

In the $T_{1\rho}$-weighted imaging sequence, a three-pulse cluster ($(\pi/2)_x$ – $(\text{spin-lock})_y$ – $(\pi/2)_{-x}$ – gradient crusher) prepares the $T_{1\rho}$-weighted magnetization. Briefly, the first $(\pi/2)_x$ pulse flips the longitudinal magnetization into the transverse plane along the y-axis. Then a long low power pulse is applied along the y-axis to spin-lock the magnetization. The second $(\pi/2)_{-x}$ pulse flips this spin-locked magnetization back to the z-axis. Residual transverse magnetization is then dephased by a crusher gradient. Magnetization stored along the z-axis is then read out by a fast spin echo (FSE) sequence (28). Imaging parameters were: echo train length (ETL) = 4, TR = 4 sec, FOV = 7 × 7 cm, slice thickness = 3 mm, matrix size = 512 × 128, NEX = 1, total scan time = 2.08 min. For a fixed spin-lock frequency, a series of $T_{1\rho}$-weighted images were obtained with varying spin-lock length (TSL) from 23–123 ms. The spin-lock frequency was calibrated from the amplitude and length of the hard 90° pulse employed. The typical length of the hard 90° pulse was 100 μs. The spin-lock field was varied from 0–1500 Hz.

Patellae were stored frozen for histology and PG quantitation after the MR experiments were completed. After thawing, 5 mm discs were cored from both sides of each patella and fixed in 10% formalin for histology. The remaining portion of the cartilage was pried from the bone with a cartilage knife and digested in papain. PG assays were performed on the papain-digested media (27). Total PG in the tissue was computed as the sum of the PG calculated from the trypsin and papain-digested solutions. The formalin-fixed discs were decalcified and embedded in paraffin wax. They were then cut into slices of 5 μm thickness and stained with 0.1% aqueous safranin-O.

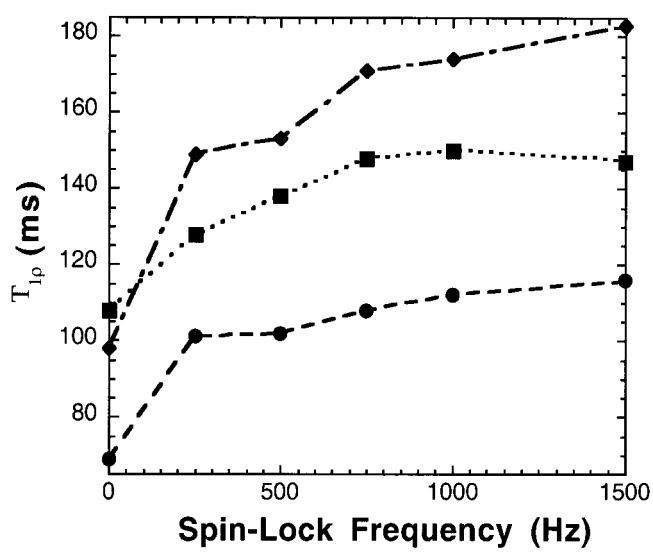

FIG. 2. $T_{1\rho}$-relaxation times of bovine cartilage are plotted against the spin-lock frequency for (●) healthy bovine cartilage, (■) 20%, and (◆) 40% PG depletion. $T_{1\rho}$ increased with B_1 in a nonlinear fashion and plateaued between 900–1000 Hz.

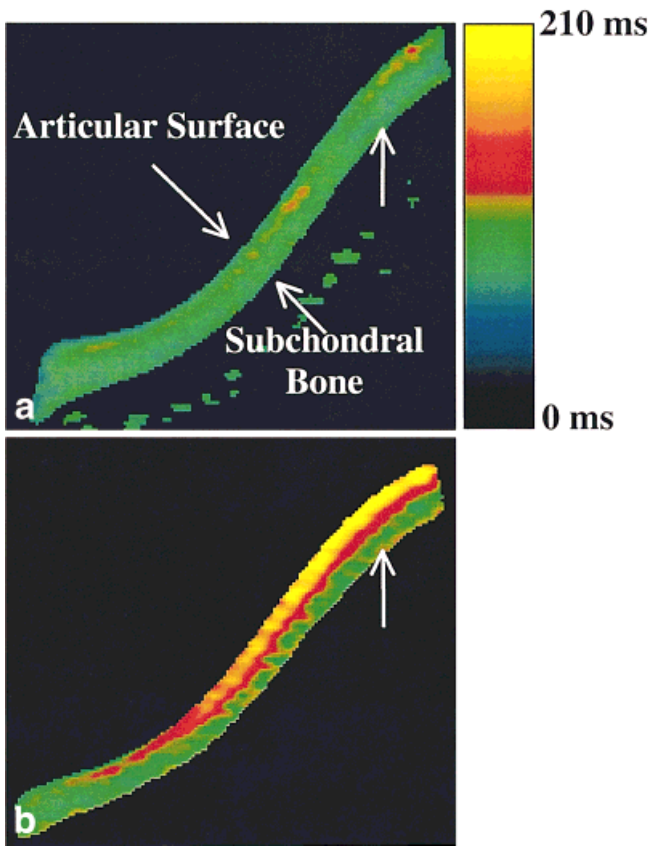

FIG. 3. $T_{1\rho}$ maps of bovine patellae. **a:** Control patella. **b:** 40% PG depleted patella. The imaging parameters were: B_1 field of 750 Hz; TR = 4 sec; FOV = 7 × 7 cm; slice thickness = 3 mm; matrix = 512 × 128; NEX = 1.

Data was processed off-line on an SGI workstation with software written in IDL language (RSI Tech., Boulder, CO). $T_{1\rho}$ maps were computed by fitting the intensity of the $T_{1\rho}$-weighted image pixel intensity as a function of length of the spin-lock pulse to the following equation (29):

$$M_y(TSL) = M_0 e^{-(TSL/T_{1\rho})} + K$$

where My, Mo, and K are the components of transverse magnetization, equilibrium magnetization, and a constant, respectively. The calculated $T_{1\rho}$ is an average of several pixels from a region of interest (ROI).

RESULTS AND DISCUSSION

Figure 1 displays T_2- and $T_{1\rho}$-weighted images of a healthy bovine patella. The images are basically featureless, with signal intensity being nearly uniform throughout the tissue. It can be seen that since $T_{1\rho}$ is longer than T_2, the $T_{1\rho}$-weighted image has a better SNR than the T_2-weighted image. The value of $T_{1\rho}$ is equal to T_2 at zero spin-locking field. Figure 2 shows plots of $T_{1\rho}$-dispersion of cartilage. From this figure it should be noted that at any given spin-lock field, the $T_{1\rho}$ values of PG-degraded cartilage are greater than that of normal cartilage. There is an increase in $T_{1\rho}$-relaxation times in PG-depleted regions, which is responsible for the higher signal intensity in the depleted

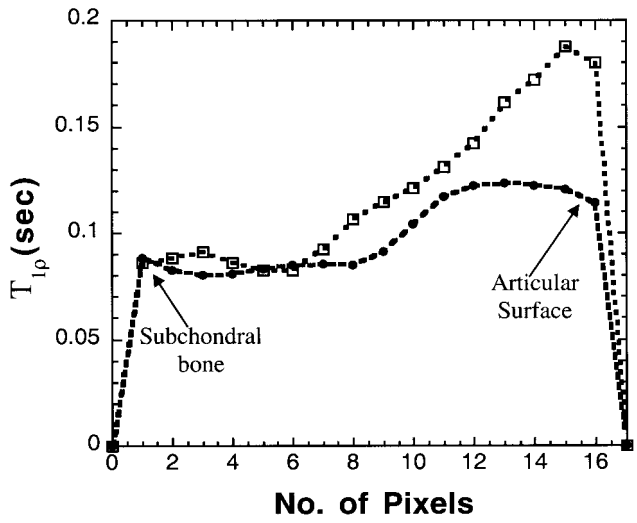

FIG. 4. The variation of $T_{1\rho}$ values across cartilage shown in maps presented in Fig. 3. Regions of the image pixels plotted are indicated by the arrows in Fig. 3. Bottom curve (●) represents data from healthy cartilage and the top curve (□) is from cartilage subjected to 40% PG depletion.

region. $T_{1\rho}$ values approached close to their maximum and plateaued between 900–1000 Hz.

The most depletion occured in the top 40–50% of the cartilage. This can clearly be seen in Fig. 3. Figure 3a represents the $T_{1\rho}$ map of a control patella and Fig. 3b is the $T_{1\rho}$ map of a patella that was subjected to ~40% PG depletion in which each pixel represents a $T_{1\rho}$-relaxation number. The higher signal intensity present in the map corresponding to the PG-depleted patella was due to the longer relaxation time of $T_{1\rho}$ compared to the map of

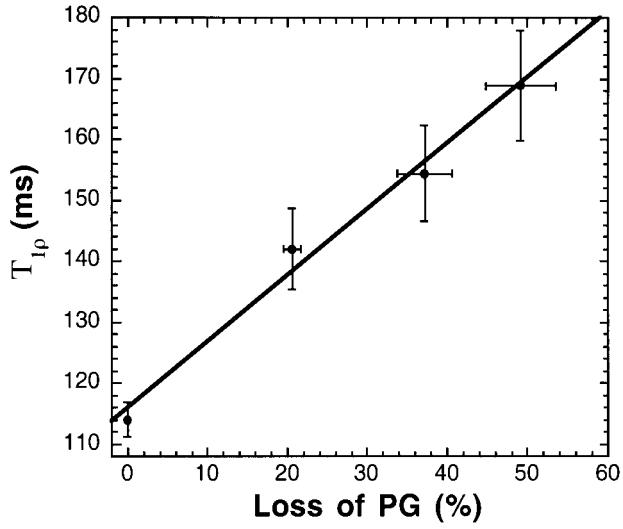

FIG. 5. PG-induced variation on $T_{1\rho}$. Each data point is an average of data obtained from five specimens. The error bars indicate SEM in the $T_{1\rho}$ and PG measurements. The solid line indicates the linear fit to the experimental data. A strong correlation (R^2 = 0.987 and slope = 1.08) between change in PG and $T_{1\rho}$ is evident. One can see that with an over 50% PG depletion, $T_{1\rho}$ increased from 110 to ~170 ms.

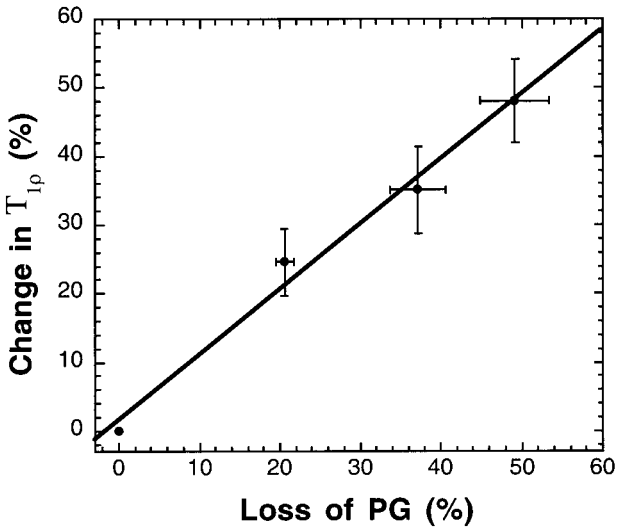

FIG. 6. Percent change in $T_{1\rho}$ vs. percent PG loss. The solid line indicates the linear fit to the experimental data. A strong correlation ($R^2 = 0.986$, slope = 0.95) between change in PG and $T_{1\rho}$ can be seen. It is evident that there is almost a linear relation between percent $T_{1\rho}$ change vs. percent PG change in cartilage.

the control cartilage. The variation of the $T_{1\rho}$ value from the subchondral bone surface towards the superficial zones at regions across cartilage (marked with arrow) is plotted against the pixel number in Fig. 4. From this figure it can be seen that the $T_{1\rho}$ value is highest in the superficial zone and decreases towards the middle zone and again shows an increasing trend near the end of the deep zone. Due to the orientation of patellar surface parallel to B_0, we did not observe trilaminar appearance in the images. However, it should be noted that in other studies on cartilage trilaminar appearance has been observed and has been attributed to the changes in dipolar interaction due to different orientations of collagen fibers in different zones of cartilage (30,31). Short water $T_{1\rho}$-relaxation times in the center of the tissue may be due in part to strong interactions with the macromolecules, with long relaxation times found in the superficial zone due to free water. Figure 5 shows the plot of $T_{1\rho}$ values obtained from the cartilage of bovine patella as a function of percent PG loss. The $T_{1\rho}$ value is also increased almost linearly as the percent loss of PG increased. Each data point is a mean ± standard error of mean (SEM) (n = 5) of values obtained from five different patellae. It should be noted that in order to minimize intersample variability we performed sequential digestions of each patella.

Figure 6 shows the percent PG loss plotted against the percent change in $T_{1\rho}$. This plot shows that over a 50% loss in PG induced a ~50% increase in $T_{1\rho}$. Regression analysis of the data shows a strong correlation ($R^2 = 0.987$) between the changes in PG and $T_{1\rho}$. This almost linear change in $T_{1\rho}$ as a function of PG loss implies that $T_{1\rho}$-imaging can be used to map the PG distribution in cartilage with all the advantages associated with proton imaging. In Fig. 7 we present representative histological sections stained for PG. The section representing depleted specimen clearly shows the region in which PG is depleted (dark red color represents normal PG content in healthy specimen). It should be noted that due to longer relaxation times this technique allows for imaging at echo times much longer than T_2 (TE+TSL). Additionally, as $T_{1\rho}$-weighted imaging deals with spin-locked magnetization, it inhibits or minimizes artifacts due to diffusion and susceptibility artifacts found at the synovial interface.

An important parameter when using $T_{1\rho}$-imaging is the specific absorption ratio (SAR) by the tissue at the B_1 fields used in the imaging experiment (32–34). From the $T_{1\rho}$-dispersion data it is clear that at any B_1 field, $T_{1\rho}$ is substantially higher than the T_2 value. With imaging parameters employed in the present study, any B_1 field at or below 750 Hz is well within the SAR requirements for human (35,36). This is the primary reason behind using the 750 Hz B_1 in the data presented in Figs. 3–6.

$T_{1\rho}$-imaging can be readily implemented on clinical scanners without any hardware modification. We believe that except for changes in the magnitude of $T_{1\rho}$ numbers,

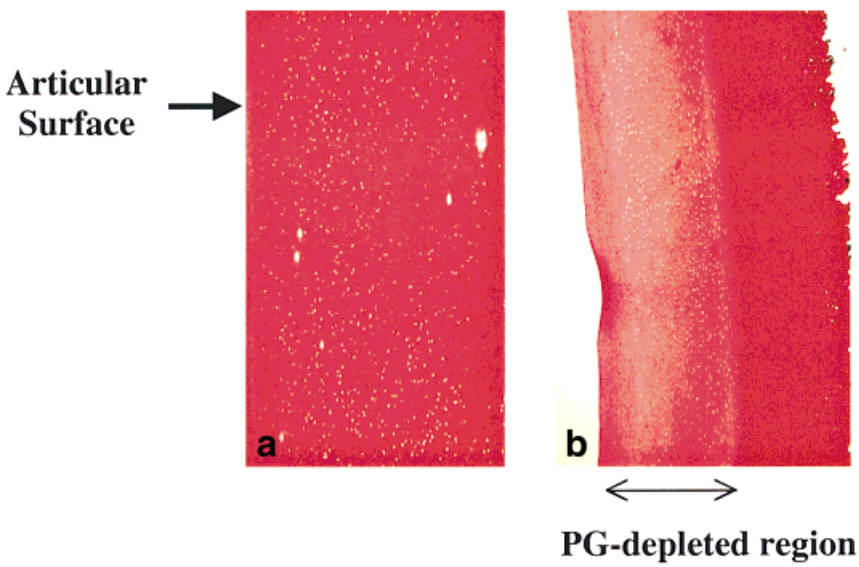

FIG. 7. Representative histological sections of bovine patellae (**a**) from a control specimen and (**b**) from the specimen subjected to ~50% PG depletion.

we expect a similar $T_{1\rho}$ behavioral trend at 1.5T. It does not require any exogenous contrast agent and $T_{1\rho}$-mapping requires relatively less imaging time than the T_1-mapping needed for dGEMRIC (17). The mechanisms responsible for $T_{1\rho}$-dispersion may involve 1) exchange of -OH protons on GAG groups and possibly on collagen with protons in H_2O; 2) exchange modulation of scalar coupling between $H_2{}^{17}O$ and $H_2{}^{16}O$; 3) exchange of protons on amino groups with water. However, in biological systems the observed $T_{1\rho}$-dispersion is due to a weighted average of these mechanisms.

These results demonstrate that $T_{1\rho}$-mapping may be exploited to sensitively measure and spatially map the changes in the PG component of articular cartilage. Specifically, as the early stages of OA involve the loss of PG with only minor changes in collagen content, $T_{1\rho}$-mapping may be potentially useful in measuring and monitoring these early degenerative changes. However, the question that needs to be answered is what is the specificity of $T_{1\rho}$ changes to PG. To address the specificity question and collagen contribution, one has to selectively deplete the collagen component and measure the $T_{1\rho}$ changes as a function of change in the collagen component. Currently, work is in progress to answer this question along with determining the underlying mechanisms contributing to the observed $T_{1\rho}$ behavior.

REFERENCES

1. Hodgeson RJ, Carpenter TA, Hall LD. Articular cartilage and osteoarthritis. New York: Raven; 1991.
2. Shapiro EM, Borthakur A, Kaufman JH, Leigh JS, Reddy R. Water distribution patterns inside bovine articular cartilage as visualized by 1H magnetic resonance imaging. Osteoarthritis Cartilage (in press).
3. Mankin HJ, Brandt KD. Biochemistry and metabolism of articular cartilage in osteoarthritis. In: Moskowitz RW, Howell DS, Goldberg VM, Mankin HJ, editors. Osteoarthritis: diagnosis and medical/surgical management. Philadelphia: W.B. Saunders; 1992. p 109–154.
4. Maroudas A. Physicochemical properties of articular cartilage. In: Freeman MAR, editor. Adult articular cartilage. Kent, UK: Pitman Medical; 1979. p 215–290.
5. Carney SL, Muir H. The structure and function of cartilage proteoglycans. Physiol Rev 1988;68:858–910.
6. Bayliss MT, Venn M, Maroudas A, Ali SY. Structure of proteoglycans from different layers of human articular cartilage. Biochem J 1983;209: 387–400.
7. Roughley PJ, Lee ER. Cartilage proteoglycans: structure and potential functions. Microsc Res Tech 1994;28:385–397.
8. Maroudas A, Muir H, Wingham J. The correlation of fixed negative charge with glycosaminoglycan content of human articular cartilage. Biochim Biophys Acta 1969;177:492–500.
9. Maroudas A, Thomas H. A simple physicochemical micromethod for determining fixed anionic groups in connective tissue. Biochim Biophys Acta 1970;215:214–216.
10. Lesperance LM, Gray ML, Burstein D. Determination of fixed charge-density in cartilage using nuclear-magnetic-resonance. J Orthop Res 1992;10:1–13.
11. Grushko G, Schneiderman R, Maroudas A. Some biochemical and biophysical parameters for the study of the pathogenesis of osteoarthritis: a comparison between the processes of ageing and degeneration in human hip cartilage. Connect Tiss Res 1989;19:149–176.
12. Lohmander LS. Articular cartilage and osteoarthrosis. The role of molecular markers to monitor breakdown, repair and disease. J Anat 1994;184:477–492.
13. Kim DK, Ceckler TL, Hascall VC, Calabro A, Balaban RS. Analysis of water-macromolecule proton magnetization transfer in articular cartilage. Magn Reson Med 1993;29:211–215.
14. Bacic G, Liu KJ, Goda F, Hoopes PJ, Rosen GM, Swartz HM. MRI contrast enhanced study of cartilage proteoglycan degradation in the rabbit knee. Magn Reson Med 1997;37:764–768.
15. Lehner KB, Rechl HP, Gmeinwieser JK, Heuck AF, Lukas HP, Kohl HP. Structure, function, and degeneration of bovine hyaline cartilage: assessment with MR imaging in vitro. Radiology 1989;170:495–499.
16. Gray ML, Burstein D, Lesperance LM, Gehrke L. Magnetization transfer in cartilage and its constituent macromolecules. Magn Reson Med 1995;34:319–325.
17. Burstein D, Velyvis J, Scott KT, Stock KW, Kim Y-J, Jaramillo D, Boutin RD, et al. Protocol issues for delayed Gd(DTPA)2-enhanced MRI (dGEMRIC) for clinical evaluation of articular cartilage. Magn Reson Med 2001;45:36–41.
18. Bashir A, Gray ML, Burstein D. Gd-DTPA2 as a measure of cartilage degradation. Magn Reson Med 1996;36:665–673.
19. Shapiro EM, Borthakur A, Dandora R, Kriss A, Leigh JS, Reddy R. Sodium visibility and quantitation in intact bovine articular cartilage using high field 23Na MRI and MRS. J Magn Reson 2000;142:24–31.
20. Reddy R, Insko EK, Noyszewski EA, Dandora R, Kneeland JB, Leigh JS. Sodium MRI of human articular cartilage in vivo. Magn Reson Med 1998;39:697–701.
21. Stanisz GJ, Henkelman RM. Gd-DTPA relaxivity depends on macromolecular content. Magn Reson Med 2000;44:665–667.
22. Sepponen RE, Pohjonen JA, Sipponen JT, Tanttu JI. A method for T1 rho imaging. J Comput Assist Tomogr 1985;9:1007–1011.
23. Santyr GE, Henkelman RM, Bronskill MJ. Spin locking for magnetic resonance imaging with application to human breast. Magn Reson Med 1989;12:25–37.
24. Duvvuri U, Reddy R, Patel SD, Kaufman JH, Kneeland JB, Leigh JS. $T_{1\rho}$-relaxation in articular cartilage: effects of enzymatic degradation. Magn Reson Med 1997;38:863–867.
25. Mlynarik V, Trattnig S, Huber M, Zembsch A, Imhof H. The role of relaxation times in monitoring proteoglycan depletion in articular cartilage. J Magn Reson Imaging 1999;10:497–502.
26. Borthakur A, Shapiro EM, Beers J, Kudchodkar S, Kneeland JB, Reddy R. Sensitivity of MRI to proteoglycan depletion in cartilage: comparison of sodium and proton MRI. Osteoarthritis Cartilage 2000;8:288–293.
27. Farndale RW, Sayers CA, Barrett AJ. A direct spectrophotometric microassay for sulfated glycosaminoglycans in cartilage cultures. Connect Tiss Res 1982;9:247–248.
28. Reddy R, Stolpen AH, Leigh JS. Detection of 17O by proton T1 rho dispersion imaging. J Magn Reson B 1995;108:276–279.
29. Rommel E, Kimmich R. Volume-selective determination of the spin-lattice relaxation time in the rotating frame T1 rho, and T1 rho imaging. Magn Reson Med 1989;12:209–218.
30. Grunder W, Wagner M, Werner A. MR-microscopic visualization of anisotropic internal cartilage structures using the magic angle technique. Magn Reson Med 1998;39:376–382.
31. Xia Y. Relaxation anisotropy in cartilage by NMR microscopy (μMRI) at 14-μm resolution. Magn Reson Med 1998;39:941–949.
32. Santyr GE, Fairbanks EJ, Kelcz F, Sorenson JA. Off-resonance spin locking for MR imaging. Magn Reson Med 1994;32:43–51.
33. Fairbanks EJ, Santyr GE, Sorenson JA. One-shot measurement of spin-lattice relaxation times in the off-resonance rotating frame using MR imaging, with application to breast. J Magn Reson Ser B 1995;106:279–283.
34. Cornell B, Pope J. A pulsed NMR study of nuclear spin-lattice relaxation in the off-resonance rotating frame. J Magn Reson 1974;16:172–181.
35. Collins CM, Li S, Smith MB. SAR and B1 field distributions in a heterogeneous human head model within a birdcage coil. Specific energy absorption rate. Magn Reson Med 1998;40:847–856.
36. Charagundla SR. Indirect 17O detection with proton magnetic resonance imaging. Ph.D. thesis, University of Pennsylvania, 2000.